Dissipative Quantum Sensing with a Magnetometer Based on Nitrogen-Vacancy Centers in Diamond

Yijin Xie,[1,2,3] Jianpei Geng,[4] Huiyao Yu,[1,2,3] Xing Rong,[1,2,3,*] Ya Wang,[1,2,3] and Jiangfeng Du[1,2,3,†]

[1] *Hefei National Laboratory for Physical Sciences at the Microscale and Department of Modern Physics, University of Science and Technology of China, Hefei 230026, China*

[2] *CAS Key Laboratory of Microscale Magnetic Resonance, University of Science and Technology of China, Hefei 230026, China*

[3] *Synergetic Innovation Center of Quantum Information and Quantum Physics, University of Science and Technology of China, Hefei 230026, China*

[4] *3. Physikalisches Institut, University of Stuttgart, Pfaffenwaldring 57, 70569 Stuttgart, Germany*

(Received 25 July 2019; revised 24 April 2020; accepted 8 June 2020; published 6 July 2020)

Quantum sensing uses quantum systems as sensors to capture weak signals and is providing opportunities in science and technology. The biggest challenge in quantum sensing is decoherence due to the coupling between the sensor and the environment. The dissipation will destroy the quantum coherence and reduce the performance of the sensor. Here we show that quantum sensing can be realized under dissipation by engineering the steady state of the sensor. We demonstrate this protocol with a magnetometer based on ensemble nitrogen-vacancy centers in diamond, while neither high-quality initialization or readout of the sensor nor sophisticated dynamical decoupling sequences are required. Thus our method provides a concise and decoherence-resistant means of quantum sensing. The frequency resolution and precision of our magnetometer are far beyond the coherence time of the sensor. Furthermore, we show that the dissipation can be engineered to improve the performance of our sensor. By increasing the laser pumping, magnetic signals in a broad audio-frequency band from dc up to 140 kHz can be tackled by our method. Besides the potential applications in magnetic sensing and imaging on the microscopic scale, our results may provide opportunities for improvement of a variety of high-precision spectroscopies based on other quantum sensors.

DOI: 10.1103/PhysRevApplied.14.014013

I. INTRODUCTION

Quantum sensing uses a quantum system to perform a measurement of a physical quantity, and it allows one to gain advantages over its classical counterpart [1]. There are a variety of quantum systems for quantum sensing, such as neutral atoms [2], trapped ions [3,4], solid-state spins [5], and superconducting circuits [1]. The regular procedure of quantum sensing includes three elementary steps: (i) initialize the state of the sensor to a superposition state; (ii) let the sensor interact with the target field; (iii) readout of the final state of the sensor. For steps (i) and (iii), high-quality and efficient initialization and readout are required. Step (ii) is usually very fragile, due to the inevitable interactions between the sensor and the environment. To minimize the effect of environmental noise, exquisite dynamical decoupling technologies have been developed to suppress the noise [6] and enhance the performance of the sensor [5]. However, the decoherence sets an upper bound on the time delay between the pulses in the dynamical decoupling sequence, corresponding to a lower bound of the detectable frequency of a signal. As a result, the detection of a low-frequency magnetic field, which is important in magnetic navigation [7,8], magnetic-anomaly detection [8], and biomagnetic field detection [9–11], can hardly benefit from the dynamical decoupling protocols.

Inspired by recent progress in dissipative quantum computation and quantum metrology [12–14], we propose and experimentally demonstrate a dissipative-quantum-sensing protocol for detection of low-frequency signals in an important type of solid-state sensor, nitrogen-vacancy (N-V) centers in diamond [15]. Because of the atomic scale of N-V centers, quantum sensing based on N-V centers provides exciting quantum technologies, such as nuclear magnetic resonance and magnetic resonance imaging at the nanoscale. An ensemble of electron spins in the form of N-V centers is used as a sensor for magnetic field measurement. The steady state of the sensor under dissipation can be engineered to be sensitive to the detected magnetic field. We show that the frequency resolution and precision go far beyond the spin coherence time. Furthermore, the

*xrong@ustc.edu.cn
†djf@ustc.edu.cn

laser-pumping procedure, during which the sensor can be initialized and read out, can be used to introduce an additional dissipation to the sensor. We also show that such a laser-controlled dissipation can increase the detection bandwidth of the sensor. Our method is capable of detecting magnetic signals over a broad audio-frequency band ranging from dc to 140 kHz.

II. EXPERIMENTAL METHOD AND SETUP

Figure 1(a) shows a schematic of the N-V center, which is an atomic defect consisting of a substitutional nitrogen and a vacancy adjacent to it. It is negatively charged since the center comprises six electrons, two of which are unpaired. The energy-level diagram is shown in the right panel in Fig. 1(a). The electronic ground state is a spin triplet state $^3A_2$ consisting of three spin sublevels $|m_s = 0\rangle$, $|m_s = +1\rangle$, and $|m_s = -1\rangle$. The N-V center can be excited from the ground state $^3A_2$ to the excited state ^3E by a laser with a wavelength of 532 nm, and decays back to the $^3A_2$ state, producing photoluminescence. The

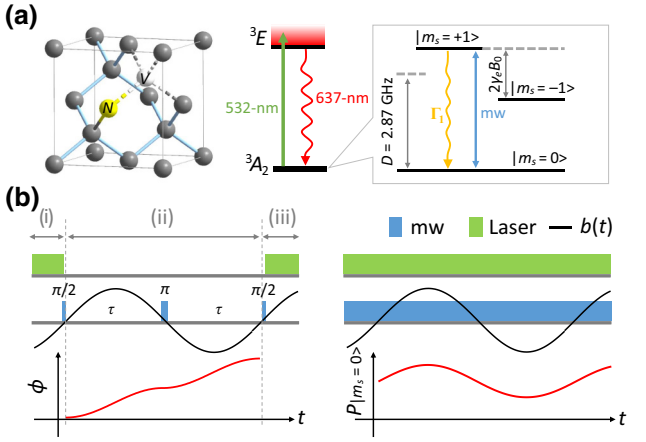

FIG. 1. Two types of quantum sensing based on N-V centers. (a) The diamond-crystal lattice with an N-V defect center is shown on the left. The energy-level diagram of the N-V center is shown on the right. The ground and excited states are denoted as $^3A_2$ and ^3E. The spin triplet $^3A_2$ contains three spin sublevels $|m_s = 0\rangle$, $|m_s = +1\rangle$, and $|m_s = -1\rangle$. The states $|m_s = 0\rangle$ and $|m_s = +1\rangle$ are encoded as the sensor. The state of the sensor can be initialized and read out with 532-nm laser pulses, and can be manipulated with microwave (mw) pulses. The initialization with laser pulses can be considered as a dissipative process in which the population decays from $|m_s = +1\rangle$ to $|m_s = 0\rangle$ with rate Γ_1. (b) The regular procedure for quantum sensing is shown on the left, with the accumulated relative phase shift ϕ as a function of time t at the bottom. Quantum sensing with steady states is shown on the right. Laser and microwave fields are continuously applied to the N-V center. The dynamics of steady states can be continuously monitored by measuring the population of state $|m_s = 0\rangle$, as shown at the bottom.

laser-induced excitation and radiative decay are spin preserving. Besides the radiative decay, there is a nonradiative decay through a metastable state, called the "intersystem-crossing process" [16]. The ionization or recombination process [17] occurs in the N-V centers during the laser pumping. The process could lead to the charge-state interconversion of N-V centers and has an impact on the dissipation effect. If we consider a round of the optical transition, there is effectively a dissipation from $|m_s = +1\rangle$ and $|m_s = -1\rangle$ to $|m_s = 0\rangle$ with decay rate Γ_1 induced by the laser. The decay rate Γ_1 is dependent on the power of the laser and thus can be harnessed by controlling the power of the laser. The optical transitions can be used for initialization of the spin state. Readout of the spin state is realized by measuring the photoluminescence intensity, since the photoluminescence intensity is contributed only by the radiative decay and shows a difference dependent on the spin state. The spin states $|m_s = 0\rangle$ and $|m_s = +1\rangle$ of the ground state $^3A_2$ are encoded as a sensor. This sensor can be manipulated by a microwave field with angular frequency $\omega_e = D - \gamma_e B_0$, where $D = 2\pi \times 2.87$ GHz is the ground-state zero splitting, $\gamma_e = -2\pi \times 28$ GHz/T is the gyromagnetic ratio of the electron spin, and B_0 is the controllable external magnetic field generated by a pair of coils.

The left panel in Fig. 1(b) presents the regular procedure for quantum sensing based on a N-V center. In step (i), a laser pulse together with a $\pi/2$ microwave pulse are applied to the N-V center to prepare the sensor in the superposition state $(|0\rangle - i|1\rangle)/\sqrt{2}$. In step (ii), we let the sensor interact with the magnetic signal. The magnetic signal contributes to a relative phase shift ϕ of the sensor state. A spin-echo technique is used to prolong the coherence time of the sensor. A π pulse is applied to decouple the interaction between the sensor and the environmental noise. If the magnetic signal is in phase with the spin-echo pulse sequence, the relative phase shift ϕ due to the magnetic signal is accumulated rather than canceled as shown at the bottom of the left panel in Fig. 1(b). More-sophisticated dynamical decoupling sequences can be applied instead of a spin-echo sequence to increase the coherence time of the N-V center. Once the coherence time is prolonged, the accumulated phase shift ϕ increases and the sensitivity will be increased [18]. The information regarding ϕ can be extracted in step (iii), which involves a $\pi/2$ microwave pulse and a laser pulse. The lowest frequency of the detected signal is bounded by $1/2\tau$ [19], where τ is the delay time between microwave pulses. However, this delay time is limited by spin decoherence, so detection of low-frequency signals by this method is challenging. Furthermore, once multiple-pulse dynamical decoupling sequences are applied, imperfection of dynamical decoupling pulses contributes to the reduction of sensitivity. The nonideal initialization and readout of the N-V center also contribute to the reduction of the observed signal.

The right panel in Fig. 1(b) shows the basic idea of our dissipative-quantum-sensing protocol. Continuous-wave laser and microwave fields are applied simultaneously during the detection procedure. The laser-induced dissipation from $|m_s = +1\rangle$ to $|m_s = 0\rangle$ can be described by an amplitude-damping process. The microwave field drives the electron spin continuously, corresponding to the evolution of the sensor governed by the Hamiltonian $H = \Delta S_z - \gamma_e b(t) S_z - \gamma_e B_1 S_x$. Here the detuning $\Delta \equiv \omega_e - \omega_{\rm mw}$ is the difference between the transition angular frequency of the electron spin ω_e and the angular frequency of the microwave field $\omega_{\rm mw}$, B_1 corresponds to the strength of the microwave field, $b(t)$ stands for the ac magnetic field to be detected along the N-V axis, and $S_x = \sigma_x/2$, and $S_z = \sigma_z/2$ are the spin operators, with σ_x and σ_z being the Pauli operators. The ac magnetic field provided by the other single coil can be written as $b(t) = b_{\rm ac}\cos(\omega_{\rm ac} t + \phi_{\rm ac})$, where $b_{\rm ac}$, $\omega_{\rm ac}$, and $\phi_{\rm ac}$ are the amplitude, angular frequency, and phase, respectively. Besides the dissipation introduced by the laser pumping, the sensor undergoes dephasing due to the interaction with environment (e.g., the nuclear-spin bath). The dephasing, with dephasing rate Γ_2, can be described by a phase-damping process. The master equation, which describes the dynamics of the state ρ of the sensor in a rotating frame, can be written as

$$\frac{d\rho}{dt} = -i[H,\rho] + \sum_{j=1,2}(2L_j \rho L_j^\dagger - L_j^\dagger L_j \rho - \rho L_j^\dagger L_j). \quad (1)$$

The first term on the right-hand side of Eq. (1) stands for the evolution under the Hamiltonian H. The second term on the right-hand side of Eq. (1) describes the dissipation process of the system. The operator $L_1 = \sqrt{\Gamma_1/2}\sigma_-$ corresponds to the amplitude damping, and $L_2 = \sqrt{\Gamma_2}/2\sigma_z$ corresponds to the phase damping [20], where $\sigma_- = (\sigma_x - i\sigma_y)/2$. Typically, the dissipation, which limits the bandwidth of the sensor in the steady-state scheme, is caused by the spin-lattice interaction. This leads to the intrinsic relaxation between ground states $|m_s = \pm 1\rangle$ and $|m_s = 0\rangle$. Here, the intrinsic longitudinal relaxation of the sensor is ignored, since the intrinsic relaxation time (about 3.9 ms) is much longer than the decay time under laser pumping ($1/\Gamma_1$, about several microseconds). The effect of laser-induced dissipation is described by the operator L_1. The dissipation process leads the sensor to a steady state. The characteristic time to reach the steady state depends on two parameters: the dephasing time under the laser, $T_2^* = 1/(\Gamma_2 + \Gamma_1/2)$, which is measured to be about 200 ns, and the decay time of amplitude damping, $T_1 = 1/\Gamma_1$.

For detection of low-frequency signals, the ac magnetic field to be detected varies in a way that is much slower than the time for the sensor to reach the steady state. In this case, the ac magnetic field can be considered quasistatic, and the state of the sensor can be approximated by the steady state under the quasistatic magnetic field.

For weak-signal detection (i.e., $|\gamma_e b(t) T_2^*| \ll 1$), the steady state ρ can be approximated, up to first order, as

$$\rho = \rho_0 + Kb(t), \quad (2)$$

where ρ_0 and $Kb(t)$ stand for the time-independent part and the time-dependent part of the steady state, respectively. ρ contains nondiagonal elements, which are sensitive to the external magnetic field. Detailed information on ρ, ρ_0, and K is provided in Supplemental Material [21].

The ac magnetic field to be detected is encoded into the state of the sensor in a linear fashion according to Eq. (2). Since the laser is applied to the N-V centers continuously, the photoluminescence intensity, which reflects the probability of the state in $|m_s = 0\rangle$ can be continuously monitored. The probability in $|m_s = 0\rangle$ is

$$P_{|m_s=0\rangle} = \frac{2 + s + 2\Delta^2 T_2^{*2}}{2(1 + s + \Delta^2 T_2^{*2})} - \frac{\gamma_e \Delta T_2^{*2} s}{(1 + s + \Delta^2 T_2^{*2})^2} b(t), \quad (3)$$

where $s = \gamma_e^2 B_1^2 T_1 T_2^*$. The dynamics of the probability $P_{|m_s=0\rangle}$ is plotted schematically at the bottom of the right panel in Fig. 1(b). The oscillation of $P_{|m_s=0\rangle}$ reflects the amplitude and frequency of the ac magnetic field $b(t)$. When the detuning Δ is set to $\sqrt{1+s}/\sqrt{3}T_2^*$, the optimal sensitivity for signal detection is reached. Since ρ is a steady state that can last for arbitrary long time, the detection can be, in principle, of arbitrary precision.

An experimental setup [21] is developed for a magnetometer based on an ensemble of N-V centers. Continuous-wave laser and microwave fields are applied to the N-V centers. The microwave field is fed to the N-V centers by a double split-ring resonator. B_0 is generated by a pair of coils with a programmable dc power supply (DP832, RIGOL Technologies). A single coil is used to send the magnetic field $b(t)$ to N-V centers. The waveform of $b(t)$ is generated by a wave generator (33500B, Keysight Technologies). Two photodiodes (PDA36A, Thorlabs) are used to transform the intensities of the green laser and red fluorescence to voltages, which can be monitored by a two-channel lock-in amplifier (HF2LI, Zurich Instruments). The time constant of the lock-in amplifier is set to zero when it is used as an oscilloscope. The voltage, v_1, from photodiode 1, which receives the red fluorescence, is proportional to the probability $P_{|m_s=0\rangle}$ of state in $|m_s = 0\rangle$. The voltage, v_2, from photodiode 2, which receives the green laser, is used to cancel the long time drift due to the laser-power instability.

III. RESULTS AND DISCUSSION

Figure 2(a) shows the experimental data for v_1, which reflects $P_{|m_s=0\rangle}$ of the steady state, as a function of time when the frequency of $b(t)$ is set to 9 Hz. The voltage v_1 is

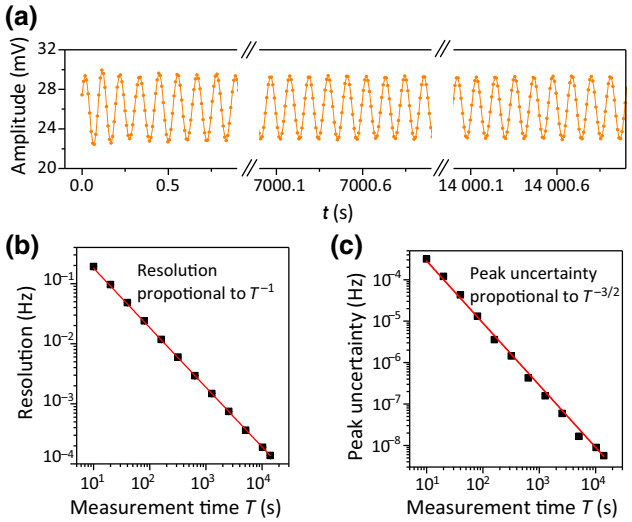

FIG. 2. Experimental frequency resolution and precision measurement. (a) Experimental data for detection of a 9-Hz magnetic field. The voltage reflects the population in $|m_s = 0\rangle$ of the sensor state. A coherent oscillation that lasts for about 4 h without decay is observed, showing that the sensor is in a steady state. (b) Frequency resolution as a function of total measurement time T. The solid line indicates that the resolution increases with the measurement time T as T^{-1}. (c) Precision of frequency estimation as a function of the measurement time T. The solid line indicates that the precision increases with the measurement time as $T^{-3/2}$.

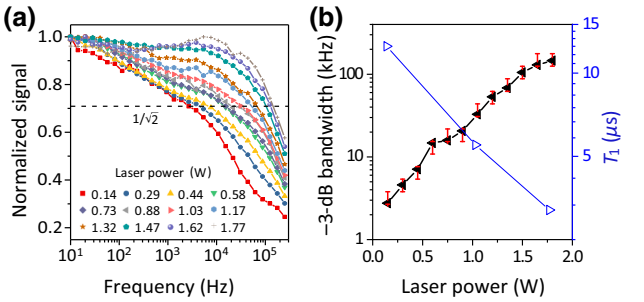

FIG. 3. Experimental measurement of the detection bandwidth. (a) The normalized measured amplitudes of v_1 as a function of the frequency of $b(t)$ with different values of the laser power. The detection bandwidth is defined as the frequency of $b(t)$ at which the normalized amplitude decreases to $1/\sqrt{2}$. (b) The experimental detection bandwidth and T_1 as a function of the laser power. The error bars of the bandwidth come from the differences between the nearest experimental data points and $1/\sqrt{2}$.

recorded by the lock-in amplifier, which is used as an oscilloscope with the frequency of its reference signal set to zero. It can be observed that there is a coherent oscillation that lasts for about 4 h without decay. The nondecay behavior shows that the quantum state of the sensor is a steady state as expected. The ac magnetic field $b(t)$ is encoded into v_1 according to Eq. (3). The frequency of $b(t)$ is the same as that of v_1, and the amplitude of $b(t)$ is proportional to that of v_1. The fast Fourier transformation of v_1 provides the spectrum of $b(t)$ in the frequency domain. The peak position of the spectrum corresponds to the frequency of $b(t)$, and the linewidth of the spectrum is defined as the frequency resolution. The frequency and frequency resolution are obtained by our fitting the spectrum, with the fitting uncertainty of the frequency defined as the frequency precision [19,22]. Figure 2(b) shows the frequency resolution as a function of the measurement time T. The frequency resolution increases with the measurement time as T^{-1}. When the data for v_1 are measured for $T = 14\,000$ s, a frequency resolution of 138 μHz is obtained. Figure 2(c) shows the frequency precision as a function of the measurement time T. The frequency precision increases with the measurement time as $T^{-3/2}$.

Figure 3 shows the experimental measurement of the detection bandwidth for our dissipative-quantum-sensing protocol. Since the protocol is based on the steady state under a quasistatic magnetic field $b(t)$, the detection bandwidth of $b(t)$ depends on the rate at which the sensor reaches the steady state. The rate to reach the steady state can be engineered by varying the laser power, since the laser power influences the decay time T_1 of the amplitude damping. At a certain laser power, as the frequency of $b(t)$ increases, the rate at which $b(t)$ varies will be more and more comparable with the rate at which the sensor reaches the steady state. If the frequency of $b(t)$ reaches a value large enough, the assumption of quasistatic $b(t)$ will no longer hold and the quantum state of the sensor will no longer be a steady state. Therefore, the amplitude of v_1 is expected to decrease with increasing frequency of $b(t)$. In the experiment, the amplitude of v_1 is measured by the lock-in amplifier, with the frequency of its reference signal set to that of $b(t)$. Figure 3(a) shows the measured amplitudes as a function of the frequency of $b(t)$ when the laser power is set to a series of values. For clarity, the amplitudes are normalized so that their values at the first point equal 1. As expected, the normalized amplitude decreases as the frequency of $b(t)$ increases for any certain laser power. The frequency at which the normalized amplitude decreases to $1/\sqrt{2}$ is defined as the detection bandwidth. Figure 3(b) shows the detection bandwidth and T_1 as a function of the laser power. It clearly shows that the detection bandwidth increases as the laser power increases and that T_1 decreases as the laser power decreases. The relation between T_1 and the laser power indicates the dissipation can be controlled by the laser. When the laser power is set to 1.8 W, a detection bandwidth of 146 kHz is achieved. Thus, the increase of the detection bandwidth by engineering the laser power is demonstrated.

IV. CONCLUSION

In conclusion, we propose and experimentally demonstrate a dissipative-quantum-sensing protocol based on the steady state of the sensor of ensemble N-V centers in diamond. The frequency resolution and precision are far beyond the limit of the sensor's coherence time. We experimentally show that the frequency resolution and precision can be increased with the measurement time T as T^{-1} and $T^{-3/2}$, respectively. The detection bandwidth in our protocol can be engineered by controlling dissipation. As demonstrated in experiments, the detection bandwidth increases as the laser power increases. When the laser power is set to 1.8 W, detection of an ac magnetic field over a broad band ranging from dc to about 140 kHz can be achieved. In the future, the dissipation could be further optimized by considering the ionization or recombination process. Our method is essentially different from magnetic field detection by a continuous-wave method based on N-V centers [11,23], whose bandwidth is limited by the time constant of the lock-in amplifier. The sensitivity of our setup is measured to be about 1 $\mathrm{nT}/\sqrt{\mathrm{Hz}}$ when the frequency is higher than 1 kHz [21]. Although this work is not intended to obtain high sensitivity, the sensitivity can be further increased by optimizing the experimental parameters of our apparatus (e.g., the material properties of the diamond) [21]. The dynamic range of our protocol is measured to be better than 80 dB when the frequency is greater than 1 kHz [21]. A high dynamic range can be achieved with our method, because we can continuously monitor the probe and get rid of the disadvantage of the regular procedure of quantum sensing [24]. From comparison of our results with other state-of-the art results [11,19,21,22,25–30], our work achieves high-frequency resolution and a high detection bandwidth. Our protocol provides opportunities in sensing, imaging, and spectroscopies based on quantum sensors.

ACKNOWLEDGMENTS

This work was supported by the National Key R&D Program of China (Grants No. 2018YFA0306600 and No. 2016YFB0501603), the Chinese Academy of Science (Grants No. GJJSTD20170001, No. QYZDY-SSW-SLH004, and No. QYZDB-SSW-SLH005), the National Natural Science Foundation of China (Grants No. 81788101 and No. 11761131011), and the Anhui Initiative in Quantum Information Technologies (Grant No. AHY050000). X.R. thanks the Youth Innovation Promotion Association of the Chinese Academy of Sciences for support. Y. Xie and J. Geng contributed equally to this work.

[1] C. L. Degen, F. Reinhard, and P. Cappellaro, Quantum sensing, Rev. Mod. Phys. **89**, 035002 (2017).

[2] J. Kitching, S. Knappe, and E. A. Donley, Atomic sensors – a review, IEEE Sens. J. **11**, 1749 (2011).

[3] R. Maiwald, D. Leibfried, J. Britton, J. C. Bergquist, G. Leuchs, and D. J. Wineland, Stylus ion trap for enhanced access and sensing, Nat. Phys. **5**, 551 (2009).

[4] M. J. Biercuk, H. Uys, J. W. Britton, A. P. VanDevender, and J. J. Bollinger, Ultrasensitive detection of force and displacement using trapped ions, Nat. Nanotechnol. **5**, 646 (2010).

[5] J. M. Taylor, P. Cappellaro, L. Childress, L. Jiang, D. Budker, P. R. Hemmer, A. Yacoby, R. Walsworth, and M. D. Lukin, High-sensitivity diamond magnetometer with nanoscale resolution, Nat. Phys. **4**, 810 (2008).

[6] G. de Lange, Z. H. Wang, D. Ristè, V. V. Dobrovitski, and R. Hanson, Universal dynamical decoupling of a single solid-state spin from a spin bath, Science **330**, 60 (2010).

[7] W. L. Webb, Aircraft navigation instruments, Electr. Eng. **70**, 384 (1951).

[8] J. E. Lenz, A review of magnetic sensors, Proc. IEEE **78**, 973 (1990).

[9] J. Wikswo, J. Barach, and J. Freeman, Magnetic field of a nerve impulse: First measurements, Science **208**, 53 (1980).

[10] M. Hämäläinen, R. Hari, R. J. Ilmoniemi, J. Knuutila, and O. V. Lounasmaa, Magnetoencephalography—theory, instrumentation, and applications to noninvasive studies of the working human brain, Rev. Mod. Phys. **65**, 413 (1993).

[11] J. F. Barry, M. J. Turner, J. M. Schloss, D. R. Glenn, Y. Song, M. D. Lukin, H. Park, and R. L. Walsworth, Optical magnetic detection of single-neuron action potentials using quantum defects in diamond, Proc. Natl. Acad. Sci. **113**, 14133 (2016).

[12] F. Verstraete, M. M. Wolf, and J. Ignacio Cirac, Quantum computation and quantum-state engineering driven by dissipation, Nat. Phys. **5**, 633 (2009).

[13] F. Reiter, A. S. Sørensen, P. Zoller, and C. A. Muschik, Dissipative quantum error correction and application to quantum sensing with trapped ions, Nat. Commun. **8**, 1822 (2017).

[14] Y. Lin, J. P. Gaebler, F. Reiter, T. R. Tan, R. Bowler, A. S. Sørensen, D. Leibfried, and D. J. Wineland, Dissipative production of a maximally entangled steady state of two quantum bits, Nature **504**, 415 (2013).

[15] M. W. Doherty, N. B. Manson, P. Delaney, F. Jelezko, J. Wrachtrup, and L. C. L. Hollenberg, The nitrogen-vacancy colour centre in diamond, Phys. Rep. **528**, 1 (2013).

[16] M. L. Goldman, A. Sipahigil, M. W. Doherty, N. Y. Yao, S. D. Bennett, M. Markham, D. J. Twitchen, N. B. Manson, A. Kubanek, and M. D. Lukin, Phonon-Induced Population Dynamics and Intersystem Crossing in Nitrogen-Vacancy Centers, Phys. Rev. Lett. **114**, 145502 (2015).

[17] Reece P. Roberts, Mathieu L. Juan, and Gabriel Molina-Terriza, Spin-dependent charge state interconversion of nitrogen vacancy centers in nanodiamonds, Phys. Rev. B **99**, 174307 (2019).

[18] L. M. Pham, N. Bar-Gill, C. Belthangady, D. Le Sage, P. Cappellaro, M. D. Lukin, A. Yacoby, and R. L. Walsworth, Enhanced solid-state multispin metrology

using dynamical decoupling, Phys. Rev. B **86**, 045214 (2012).

[19] J. M. Boss, K. S. Cujia, J. Zopes, and C. L. Degen, Quantum sensing with arbitrary frequency resolution, Science **356**, 837 (2017).

[20] Michael A. Nielsen and Isaac Chuang, Quantum computation and quantum information, (Cambridge University Press, New York, 2002).

[21] See Supplemental Material at http://link.aps.org/supplemental/10.1103/PhysRevApplied.14.014013 for information on the instrumentation, details of the calculations, and experimental procedures.

[22] S. Schmitt, T. Gefen, F. M. Stürner, T. Unden, G. Wolff, C. Müller, J. Scheuer, B. Naydenov, M. Markham, S. Pezzagna, *et al.*, Submillihertz magnetic spectroscopy performed with a nanoscale quantum sensor, Science **356**, 832 (2017).

[23] J. M. Schloss, J. F. Barry, M. J. Turner, and R. L. Walsworth, Simultaneous Broadband Vector Magnetometry Using Solid-State Spins, Phys. Rev. Appl. **10**, 034044 (2018).

[24] G. Waldherr, J. Beck, P. Neumann, R. S. Said, M. Nitsche, M. L. Markham, D. J. Twitchen, J. Twamley, F. Jelezko, and J. Wrachtrup, High-dynamic-range magnetometry with a single nuclear spin in diamond, Nat. Nanotechnol. **7**, 105 (2012).

[25] T. Wolf, P. Neumann, K. Nakamura, H. Sumiya, T. Ohshima, J. Isoya, and J. Wrachtrup, Subpicotesla Diamond Magnetometry, Phys. Rev. X **5**, 041001 (2015).

[26] Huijie Zheng, Jingyan Xu, Geoffrey Z. Iwata, Till Lenz, Julia Michl, Boris Yavkin, Kazuo Nakamura, Hitoshi Sumiya, Takeshi Ohshima, Junichi Isoya, *et al.*, Zero-Field Magnetometry Based on Nitrogen-Vacancy Ensembles in Diamond, Phys. Rev. Appl. **11**, 064068 (2019).

[27] D. Le Sage, L. M. Pham, N. Bar-Gill, C. Belthangady, M. D. Lukin, A. Yacoby, and R. L. Walsworth, Efficient photon detection from color centers in a diamond optical waveguide, Phys. Rev. B **85**, 121202(R) (2012).

[28] Jennifer M. Schloss, John F. Barry, Matthew J. Turner, and Ronald L. Walsworth, Simultaneous Broadband Vector Magnetometry Using Solid-State Spins, Phys. Rev. Appl. **10**, 034044 (2018).

[29] Sepehr Ahmadi, Haitham A. R. El-Ella, Jørn O. B. Hansen, Alexander Huck, and Ulrik L. Andersen, Pump-Enhanced Continuous-Wave Magnetometry Using Nitrogen-Vacancy Ensembles, Phys. Rev. Appl. **8**, 034001 (2017).

[30] J. F. Barry, J. M. Schloss, E. Bauch, M. J. Turner, C. A. Hart, L. M. Pham, and R. L. Walsworth, Sensitivity Optimization for NV-Diamond Magnetometry, Rev. Mod. Phys. **92**, 015004 (2020).